Journal of
MATERIALS RESEARCH

Scanning tunneling microscopy and spectroscopy studies of single wall carbon nanotubes

Teri Wang Odom, Jin-Lin Huang, Philip Kim, Min Ouyang, and Charles M. Lieber[a)]
Harvard University, Cambridge, Massachusetts 02138

(Received 6 February 1998; accepted 3 May 1998)

Scanning tunneling microscopy and spectroscopy have been used to characterize the atomic structure and tunneling density of states of individual single wall carbon nanotubes (SWNT's) and ropes containing many SWNT's. Analysis of atomically resolved SWNT images shows that the nanotubes consist of a wide range of diameters and helicities with no one structure clearly dominant. Tunneling spectroscopy measurements made simultaneously on atomically resolved SWNT's exhibit semiconducting and metallic behavior that depend predictably on helicity and diameter. In addition the band gaps of the semiconducting tubes were also found to depend inversely on diameter. These results are compared to theoretical predictions, and the implications of these studies as well as important future directions are discussed.

I. INTRODUCTION

Currently, carbon nanotubes are the focus of intense interest worldwide. This attention to carbon nanotubes is not surprising in light of their promise to exhibit unique physical properties that could impact broad areas of science and technology, ranging from superstrong composites to nanoelectronics.[1–3] Critical to realizing the potential of carbon nanotubes will be work that defines their intrinsic mechanical and electrical properties. There has been considerable experimental and theoretical progress to this end. For example, mechanical measurements have recently demonstrated that carbon nanotubes have the largest Young's modulus of any known materials.[4,5] Direct measurements of the full stress-strain behavior of individual nanotubes have also shown that nanotubes undergo a striking elastic buckling deformation, and are exceedingly tough materials.[5] It is, however, the remarkable electronic properties of carbon nanotubes that have elicited the greatest interest.[1,6–17] For single wall carbon nanotubes (SWNT's), which consist of a single graphene sheet rolled into a seamless tube, theoretical calculations predict that both metallic and semiconducting nanotubes are possible depending only on the diameter and the helicity of the nanotube.[6–10] The ability to display fundamentally distinct electronic properties without changing the local bonding sets nanotubes apart from other nanowire materials.

The diameter and helicity of a defect-free SWNT are uniquely characterized by the roll-up vector $\mathbf{c}_h = n\mathbf{a_1} + m\mathbf{a_2} \equiv (n, m)$ that connects crystallographically equivalent sites on a two-dimensional (2D) graphene sheet, where $\mathbf{a_1}$ and $\mathbf{a_2}$ are the graphene lattice vectors and n and m are integers (Fig. 1). Electronic band structure calculations predict that the (n, m) indices determine whether a SWNT will be a metal or a semiconductor.[6–10] To first order $(n,0)$ or zigzag SWNT's should exhibit two distinct types of behavior. The nanotubes will be metals when $n/3$ is an integer, and otherwise semiconductors. As $\mathbf{c}_h$ rotates away from $(n, 0)$, chiral (n, m) SWNT's are possible with electronic properties similar to the zigzag tubes; that is, when $(2n + m)/3$ is an integer, the tubes are metallic, and otherwise semiconducting. Independent of chirality, the energy gaps of the semiconducting $(n, 0)$ and (n, m) tubes should depend inversely on diameter.[1,7,10] The finite curvature of the tubes will also lead to mixing of the π/σ bonding and π^*/σ^* antibonding orbitals on carbon. This mixing should produce small gaps in $(n, 0)$ and (n, m) metallic tubes with the magnitude of the gap depending inversely with the square of the diameter. Finally, when $\mathbf{c}_h$ rotates 30° relative to $(n, 0)$, $m = n$. The (n, n) or armchair tubes are expected to be truly metallic with band crossings at $\mathbf{k} = \pm 2/3$ of the 1D Brilluoin zone.

Scanning tunneling microscopy (STM) and scanning tunneling spectroscopy (STS) offer the potential to probe these predictions for the electronic properties of carbon nanotubes, since these techniques are capable of resolving simultaneously the atomic structure and electronic density of states of a material. Atomically resolved images of *in situ* vapor-deposited (versus arc generated) carbon structures believed to be multiwall carbon nanotubes (MWNT's) were first reported by Sattler and Ge.[18] Bias-dependent imaging[19] and STS[20] investigations of independently characterized arc generated MWNT's showed that some fraction of MWNT's produced by the arc method were semiconducting,

[a)]Correspondence should be addressed to C.M.L.
e-mail: cml@cmliris.harvard.edu

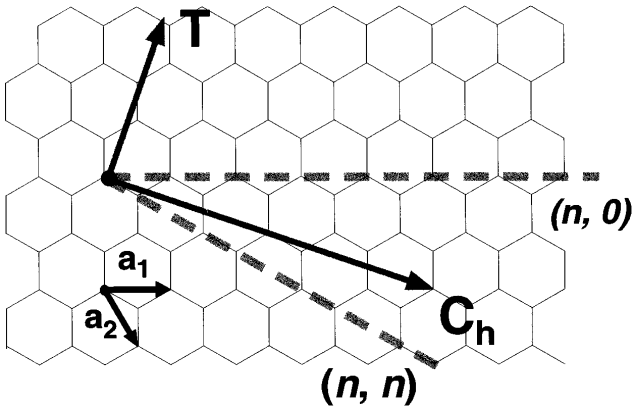

FIG. 1. Schematic of a 2D graphene sheet illustrating lattice vectors $\mathbf{a_1}$ and $\mathbf{a_2}$, and the roll-up vector $\mathbf{c}_h = n\mathbf{a_1} + m\mathbf{a_2}$. The limiting cases of $(n,0)$ zigzag and (n,n) armchair tubes are indicated with dashed lines. As represented here, the angle between the zigzag configuration and $\mathbf{c}_h$ is negative. The tube axis is indicated by the vector $\mathbf{T}$.

and furthermore, the STS data suggested that the energy gap depended inversely on diameter. Subsequent STM and STS studies of MWNT's and SWNT's have provided indications of different structures and structure-dependent electronic properties,[21–24] but have not revealed an explicit relationship between structure and electronic properties. We believe that the failure of these previous studies to elucidate clearly the expected diameter and helicity dependent electronic properties of nanotubes can be attributed in part to the lack of pure SWNT samples, since (i) the electronic band structure of MWNT's is considerably more complex than SWNT's, and (ii) relatively pure samples are required to carry out unambiguous STM and STS measurements.

The recent development of techniques to produce and purify relatively large quantities of SWNT's has made possible definitive testing of the remarkable predicted electronic properties of nanotubes.[25–27] Indeed, recent STM and STS measurements of the atomic structure and electronic properties of purified SWNT's were communicated by our group[28] and Wildoer *et al.*[29] These initial studies have shown that the electronic properties of SWNT's do indeed depend sensitively on diameter and helicity, and thus verify the major features of theory. In this paper, we describe in detail our studies of the atomic structure and electronic properties of SWNT's, including the analysis of atomic structure and nanotube indices, the types of structures present in samples prepared by current techniques, the relationship between structure and electronic properties, and issues critical to further understanding these unique materials.

II. EXPERIMENTAL METHODS

SWNT's were grown by the laser vaporization method of Thess *et al.*[25] Raw SWNT's were purified by treatment in refluxing HNO_3 followed by neutralization and filtration through a 0.8 μm pore membrane. Samples suitable for STM and STS studies were prepared by spin coating an ethanol suspension of the purified SWNT's onto Au(111) surfaces. The Au(111) films were grown by electron beam evaporation of gold onto heated (375 °C) mica; the films were annealed for 1 h at 350 °C prior to removal from the deposition chamber. Immediately after SWNT deposition onto freshly prepared Au(111) substrates, the sample was loaded into an UHV chamber and transferred under vacuum to a homemade UHV STM that was stabilized at 77 K. Large scale characterization of independent samples by atomic force microscopy (AFM) and field-emission scanning electron microscopy showed that the SWNT's consisted primarily of ropes of individual tubes distributed on the substrate surface with an average separation of approximately 10 μm (Fig. 2). STM imaging studies were carried out using electrochemically etched W tips in the constant current mode with the bias voltage (V) applied to the tip. The resolution and calibration of the STM were confirmed *in situ* by imaging the atomic lattice and steps of the Au(111) substrate surface.

STS measurements were made by averaging 5–10 I-V curves at specified locations on atomically resolved SWNT's. Typically, 6–8 distinct locations were measured for a given atomically resolved nanotube. The normalized conductance, $(V/I)dI/dV$, which has been shown to provide a good measure of major features in

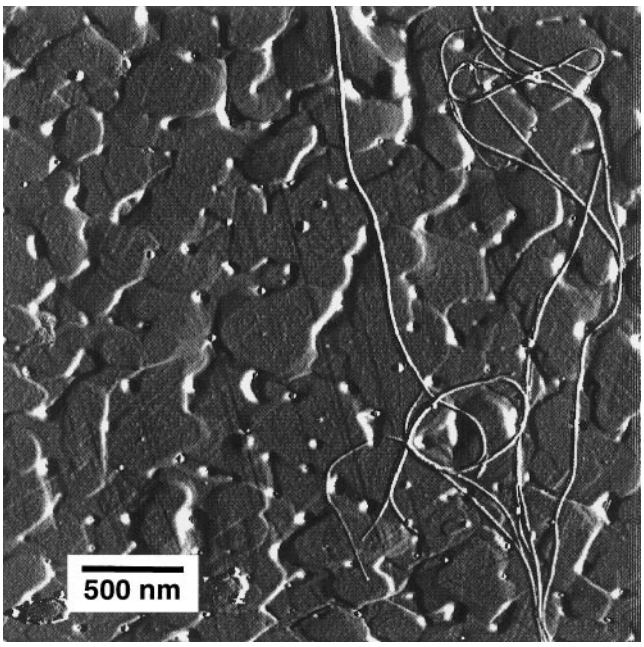

FIG. 2. Large scale AFM image of the Au(111) substrate following the deposition of SWNT's. SWNT ropes are visible as curved string-like objects several micrometers in length. The image was recorded with a Nanoscope III (Digital Instruments, Inc.) in tapping mode with a Si-FESP tip.

the local density of electronic states (LDOS) for metals and semiconductors, was calculated from digital I-V data using standard methods.[30] To ensure the reliability of these measurements, we routinely checked that clean areas of the Au(111) substrate exhibited the characteristic metallic I-V curves and the expected 2D surface state of this material.[31] In addition, we routinely checked that I varied exponentially with tip-sample separation to verify the presence of a clean vacuum tunneling junction.

The (n, m) indices of a SWNT are obtained from the experimentally determined values of the chiral angle, θ, and diameter. The chiral angle was measured between the zigzag $(n, 0)$ direction, which corresponds to sites separated by 0.426 nm along the zigzag tube axis, and the central tube axis for angles $<15°$. Because the tube axis $\mathbf{T}$ is perpendicular to $\mathbf{c}_h$, this angle is equivalent to that between the $(n, 0)$ and $\mathbf{c}_h$ directions defined in Fig. 1. When the chiral angle was $>15°$, we determined its value relative to the armchair (n, n) direction. This approach confines our angle measurements to the best defined atomic structure at the tops of the SWNT's and minimizes contributions from the structure at the sides of the highly curved tubes, since the latter can be distorted by the finite size and asymmetry of the tip. In addition, we independently determined the chiral angles from analysis of the Fourier transform of atomically resolved data; i.e., the angle between reciprocal space lattice and the tube axis. Taken together these methods yield an uncertainty in the chiral angle of $\pm 0.5°$.

SWNT diameters were determined from the projected widths of nanotube images after deconvoluting the tip contribution to the image. First, we assign an overall width by averaging ~400 cross sections for each nanotube. The total tunneling current I can then be expressed as $I = I_g \exp(-k_g z) + I_t \exp[-k_t\sqrt{x^2 + (z - R^2}]$ near the nanotube and $I = I_g \exp(-k_g d)$ far away from the nanotube, where k_g, k_t, R, and d are the inverse decay length on gold, the inverse decay length on the tube, the tube radius and distance from the gold surface, respectively. I_t and I_g contain the complicated electronic structure of both the tip and the tube. This equation is then used to fit the average cross section obtained from the STM image to obtain the nanotube diameter $2R$. The parameters obtained from this model are reasonable and are in agreement with those obtained from Au steps in the same experiments. The typical uncertainty in SWNT diameter from high-quality STM images is ± 0.05 nm. We believe that this approach yields a more robust diameter than that determined from the cross-sectional height, since the apparent height is highly dependent on the imaging conditions.

Lastly, we have also developed a projection-matching method to verify that the assigned (n, m) indices are consistent with the experimental images. A program is used to generate nanotube structures with (n, m) indices closest to the ones derived from the chiral angle and diameter analyses described above, and then a two-dimensional (2D) projection of the three-dimensional (n, m) indices is directly overlaid on an experimental image to determine the best-fit (n, m) indices. Our comparison (as above) focuses on the match at the tops of the tubes where the atomic structure is best defined. Although the fits typically have deviations, the relative fit of possible (n, m) indices usually produces one set that is clearly better than others.

III. RESULTS AND DISCUSSION

A. Nanotube structure

Typical STM images of a SWNT rope and an isolated SWNT are shown in Fig. 3. These images illustrate several general points. First, the chiral angles determined from the tubes span a wide range; for the rope in Fig. 3, the angles range from approximately $0-17°$. A wide range of helicities is typical for the rope and isolated tubes and suggests that no one structure dominates in our SWNT samples. This point is addressed further below. Second, isolated SWNT's can be observed, although we typically find these adjacent to ropes [Fig. 3(b)]. The latter observation suggests that the isolated SWNT's peel off from (and can remain connected to) the ropes. Third, large scale images often exhibit raised features on tubes [e.g., pronounced bright area in lower right of Fig. 3(b)]. These features could be due to contamination from the deposition process, variations in coupling to the substrate, or may be intrinsic to the SWNT's. Although we can confine our measurements to other sample areas, these features could influence other measurements, such as transport, carried out on SWNT samples deposited in a similar manner.

Our ability to characterize the detailed SWNT structure defined by the (n, m) indices from atomic resolution images is one major point of this paper. We illustrate this capability and limitations in assigning (n, m) indices with several specific tube examples. Typical atomically resolved images of a SWNT on the surface of a rope and isolated SWNT's on a Au(111) substrate are shown in Figs. 4 and 5, respectively. The expected honeycomb lattice for a SWNT with a C–C spacing of 0.14 ± 0.02 nm is resolved clearly in Fig. 4. The chiral angle determined by measuring the angle formed between the tube axis (solid line) and zigzag direction (dashed line) is $-8.0 \pm 0.5°$. In general, we find that the chiral angles determined at different positions along straight tubes are the same over distances of at least 20 nm, and thus we believe that twist deformations do not affect the data presented in this paper. This angle and the measured

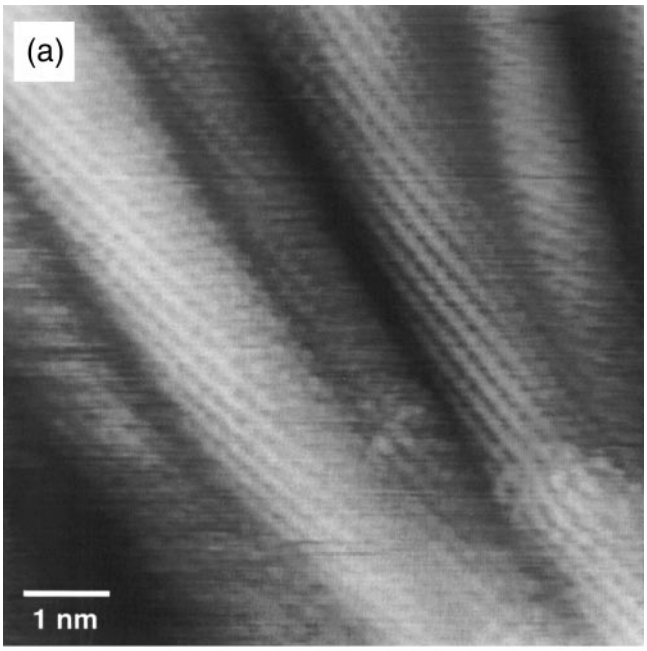

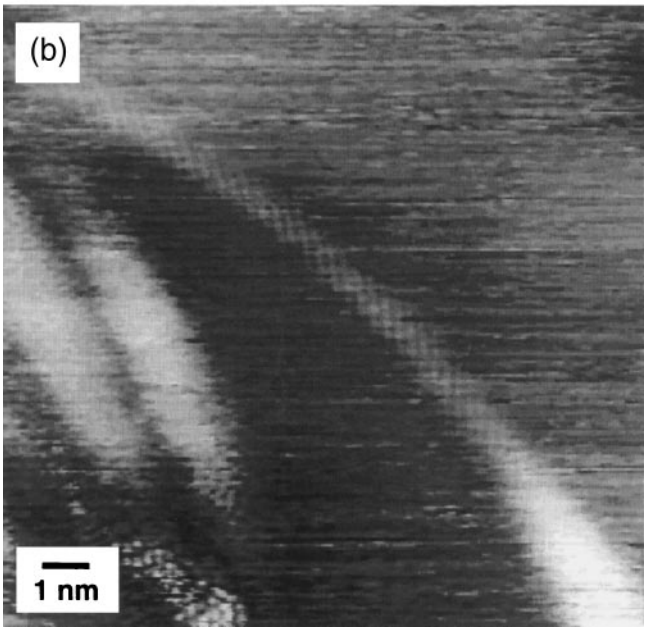

FIG. 3. STM images of (a) a SWNT rope and (b) an isolated SWNT. The atomic structure of the SWNT's is clearly visible in both images. The data in (a) and (b) were recorded in the constant current mode with a bias voltage of 250 mV and a tunneling current of 120 pA.

diameter of 1.0 ± 0.05 nm can be used to assign (n, m) indices to the SWNT. Within our uncertainty we can assign the indices to be either $(11, 2)$ or $(12, 2)$ with angles/diameters of $-8.2°/0.95$ nm and $-7.6°/1.03$ nm, respectively. Note that an $(11, 2)$ tube is expected to be metallic, while a $(12, 2)$ tube should be semiconducting.

A similar analysis has also been carried out for the isolated SWNT's. The chiral angle of the upper isolated

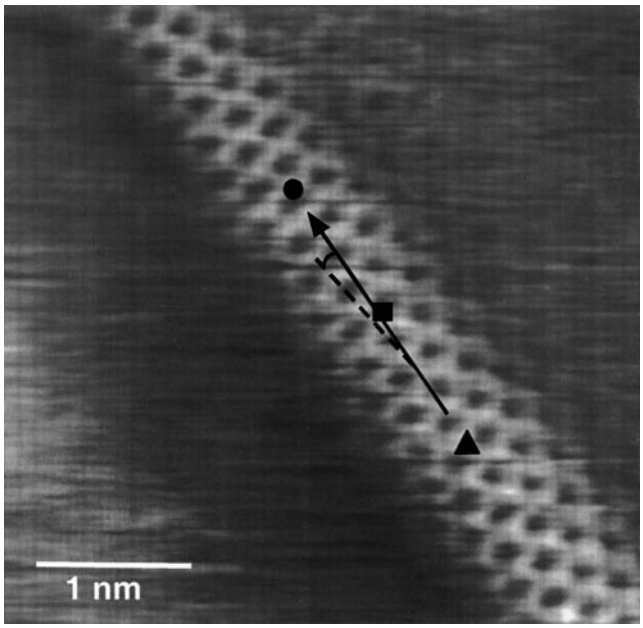

FIG. 4. STM image of a SWNT exposed at the surface of a rope on a Au(111) substrate. The image was recorded in the constant current mode with a bias voltage of 50 mV and a tunneling current of 150 pA. The image was low-pass filtered. The tube axis is indicated with solid, black arrows, and the zigzag direction is highlighted by a dashed line. The symbols correspond to the locations where *I-V* was measured. Adapted from Ref. 28.

SWNT in Fig. 5(a) was found to be $11.2 \pm 0.5°$, while the diameter of this tube is 0.95 ± 0.05 nm. Within the limits of our uncertainty either $(14, -3)$ or $(15, -3)$ indices with angle/diameter values of $11.7°/1.0$ nm and $10.9°/1.08$ nm, respectively, appear compatible with the experimental image. The lower tube in Fig. 5(a) has a similar structure. We believe that there are two possibilities for this similarity. First, the tubes could correspond to distinct isolated SWNT's. This suggestion is supported by the following: (i) it is likely that there will be a correlation in the growth and structure of adjacent tubes; (ii) it reasonable that the tubes are parallel, since they correspond to ones peeled off of a rope (and remain connected a distance away); and (iii) a larger scale image of around this area does not show doubling of other features. Alternatively, it is possible that the second tube corresponds to an image of one tube by a second tip. Although some evidence [(i)–(iii) above] contradicts this second possibility, it is difficult to distinguish unambigously between the two. The interpretation of our results is not affected by either explanation.

To constrain better the (n, m) indices of the SWNT's, we have also been exploring a new projection matching approach (see experimental methods). In brief, 2D projections corresponding to the ideal $(14, -3)$ and $(15, -3)$ tubes were calculated and then directly overlaid onto the

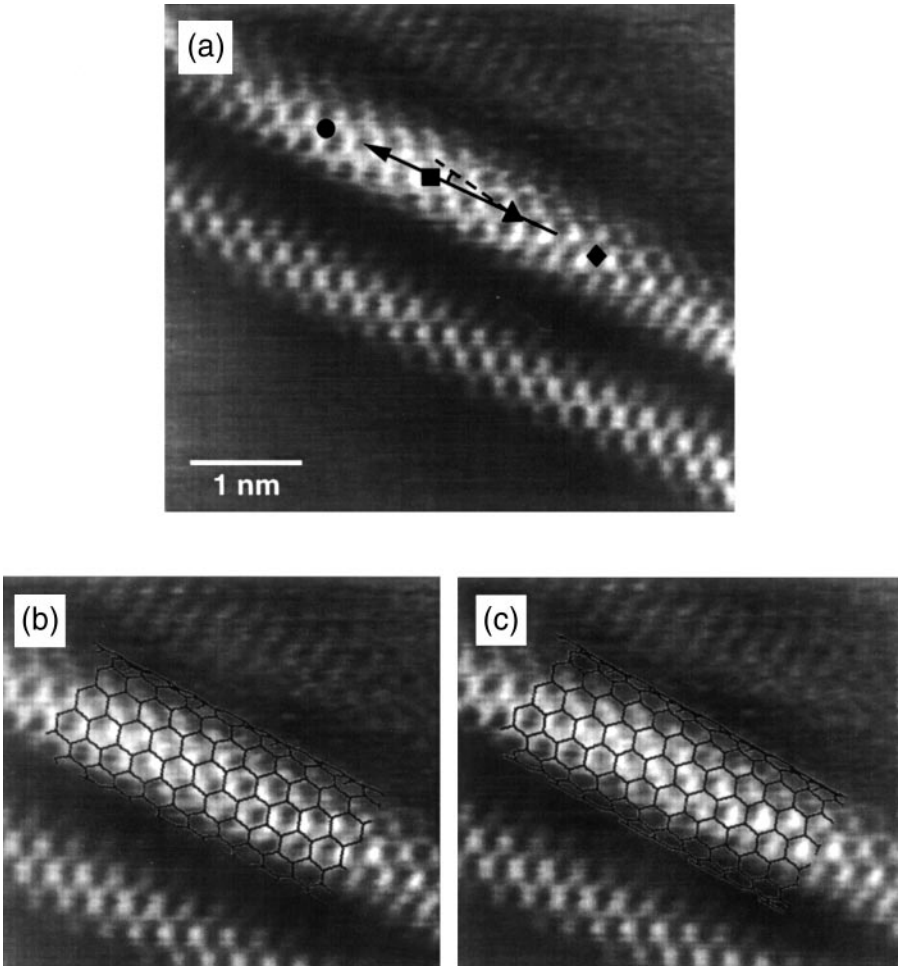

FIG. 5. (a) Constant current image of isolated SWNT's on a Au(111) surface recorded with a bias voltage of 300 mV and a tunneling current of 150 pA. The solid, black arrow highlights the tube axis, and the dashed line indicates the zigzag direction. Fits of 2D projections corresponding to (b) $(14, -3)$ and (c) $(15, -3)$ indices with the experimental data from (a). The 2D projection of a $(14, -3)$ tube matches the experimental data reasonably well over the top portion of the SWNT, while that of the $(15, -3)$ tube exhibits a large deviation over the length of the projection.

experimental image [Figs. 5(b) and 5(c)]. Comparison of the two images with overlaid projections shows that $(14, -3)$ tube better matches the experimental results at the tops of the tubes, although this match also shows deviations on the highly curved sides The advantage of this technique is that small errors or deviations, which may not be distinguishable from comparison of the angle and diameter points, propagate and become visually detectable. While we believe that this approach represents an advance over other methods used to define (n, m), it remains subject to image distortions and uncertainty in diameter (as do other approaches).

The data exhibit a richness of structures statistically favoring helicities closer toward the zigzag $(n, 0)$ direction rather than the armchair (n, n) direction. This observation contrasts previous suggestions[25,32] that SWNT's prepared by laser vaporization consist primarily of $(10, 10)$ armchair tubes. Since our STM measurements are biased toward SWNT's that have separated from outer portions of ropes, a hypothesis for this discrepancy is that SWNT ropes grow or align in such a way that armchair tubes lie at the core and are surrounded by structurally diverse tubes. Interestingly, we have observed one rope with an exposed central core (presumably exposed during the purification steps) (Fig. 6). The SWNT's in this region of the rope all exhibit well-defined armchair or (n, n)-like structures. For example, the overlaid 2D projection of a $(9, 9)$ tube exhibits an excellent fit in this image. These observations suggest that cutting and etching of the ropes may result in an enrichment of armchair tubes. Significantly, recent studies of etched SWNT's indicate a statistical shift in the helicity toward the armchair direction.[33] We believe that these results could have important implications in the growth mechanism and be very important for future applications.

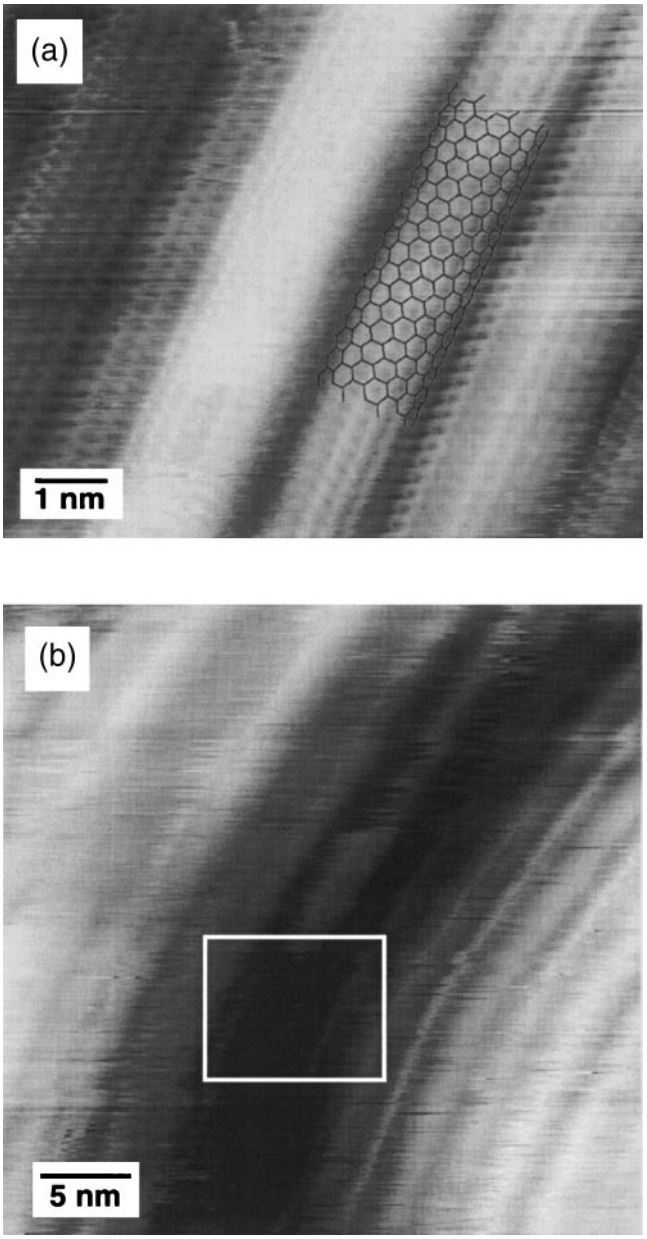

FIG. 6. (a) STM image of the central region of a SWNT rope recorded in the constant current mode with a bias voltage of 450 mV and a tunneling current of 120 pA. The SWNT's in this inner portion of the rope all exhibit armchair-like atomic structure. A 2D projection of the lattice for a (9, 9) armchair tube is shown. (b) Large-scale image illustrating the sides and exposed core of a SWNT rope. The white box highlights the core area of the rope where the image in (a) was recorded.

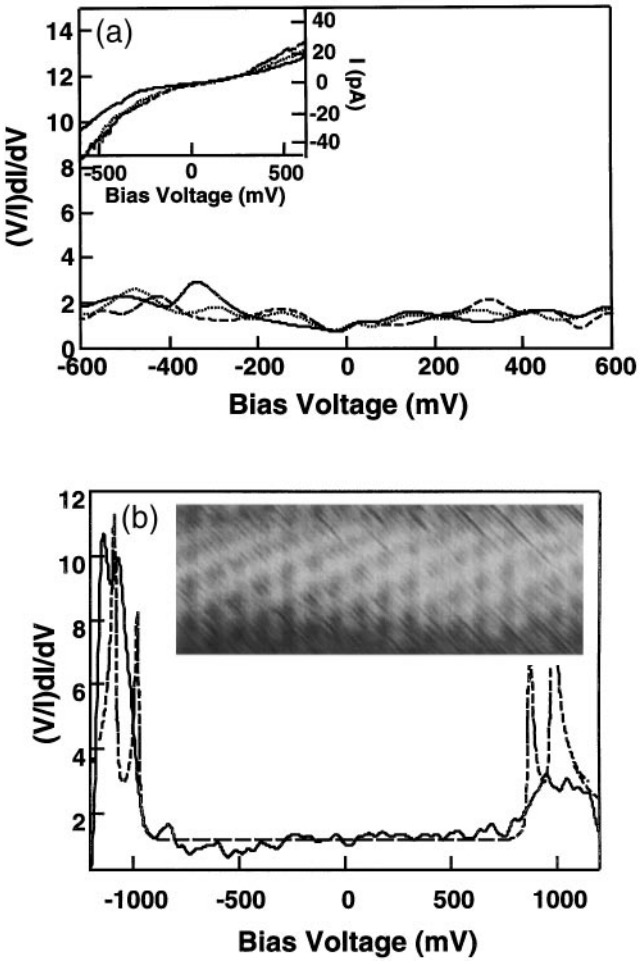

FIG. 7. Tunneling spectroscopy data recorded from the SWNT's. (a) Calculated normalized conductance, $(V/I)dI/dV$, and measured I-V (inset) from the locations indicated in Fig. 4(a): (—)/(●); (···)/(■); (- - -)/(▲). Adapted from reference 28. (b) Normalized conductance data (—) recorded on the $(15, -3)$ SWNT shown as an inset. Four similar curves were recorded at points along the tube, although only one data set is shown for clarity. The dashed curve corresponds to the DOS obtained from a tight-binding calculation for a $(15, -3)$ SWNT.[34] The calculated van Hove singularities are found to agree relatively well with the experimental data.

B. Nanotube electronic properties

Central to our investigation of SWNT's has been an ability to characterize the electronic properties of the atomically resolved tubes by tunneling spectroscopy. The gradual increase in current in the I-V data recorded on the SWNT imaged in Fig. 4 shows qualitatively that the tube is metallic [Fig. 7(a)]. The LDOS determined from data sets recorded at different locations along the tubes are very similar, demonstrating the reproducibility of the measurements. Furthermore, the LDOS for both tubes are roughly constant between -600 and $+600$ mV as expected for a metal. Small variations in LDOS with energy are not significant and arise from noise in the data. These spectroscopy results are similar to those obtained on the Au(111) substrate except that the surface state 450 meV below the Fermi level[31] is also observed on the latter.

There are several other important points that these data address. First, curvature in the graphene sheet of a SWNT should cause the π/σ bonding and π^*/σ^* antibonding orbitals on carbon to mix and create a small

gap at the Fermi level in these metallic tubes.[1,7,10] We have not observed evidence for this small gap, although it is possible that the thermal energy at 77 K, 7 meV, smears the gap structure predicted to be of order 8 meV for a (12, 0) tube.[7] However, even the 4 K study by Wildoer *et al.*[29] did not observe this mixing-induced gap. We believe that this prediction deserves further experimental and theoretical analysis. From the standpoint of experiment, it is possible that the interaction between the Au substrate and carbon nanotube obscures the predicted gap, and thus studies carried out using different substrates could illuminate this point. Second, the LDOS recorded on metallic SWNT's in a rope and isolated on the substrate are similar. These observations suggest that intertube interactions do not perturb the electronic structure on an energy scale of 77 K. Lastly, our analysis of *I-V* data recorded over an extended range of bias voltages reveals the characteristic van Hove singularities at the band edges of the 1D SWNT's. The spectroscopy data shown in Fig. 7(b) show sharp features near ± 1 eV that are consistent with these singularities. Moreover, a tight-binding calculation carried out for the assigned (15, −3) structure yields density of states peaks in reasonably good agreement with these experimental data.[34] In the future, we believe that further and more detailed comparisons of the experimentally determined and calculated electronic band structure should serve as an important test of our understanding of the SWNT materials.

We have also characterized a number of semiconducting SWNT's in our studies. Indeed, more than half of the SWNT's observed either as isolated tubes or in ropes were found to be moderate gap semiconductors. A typical example of tunneling spectroscopy data obtained from an isolated semiconducting SWNT is shown in Fig. 8(a). The *I-V* data, which were recorded on the atomically resolved tube shown in Fig. 5(a), exhibit distinctly different behavior from the metallic tubes and are consistent with a semiconductor; that is, the current is very small for $-300 < V < +400$ mV, but increases sharply when $|V|$ is increased further. The calculated $(V/I)dI/dV$ shows sharper increases at −325 and +425 mV that correspond to the conduction and valence band edges in the LDOS. These band edges exhibit the divergent behavior characteristic of and expected for the one-dimensional (1D) SWNT's. In addition, from the well-defined band edges we can define a band gap of 750 meV.

The observed semiconducting behavior is consistent with the expectation that a (14, −3) tube should be a moderate gap semiconductor [i.e., $(2n + m)/3$ is not an integer]. In addition, we have observed similar semiconducting behavior for other chiral and zigzag tubes characterized with atomic resolution. A summary

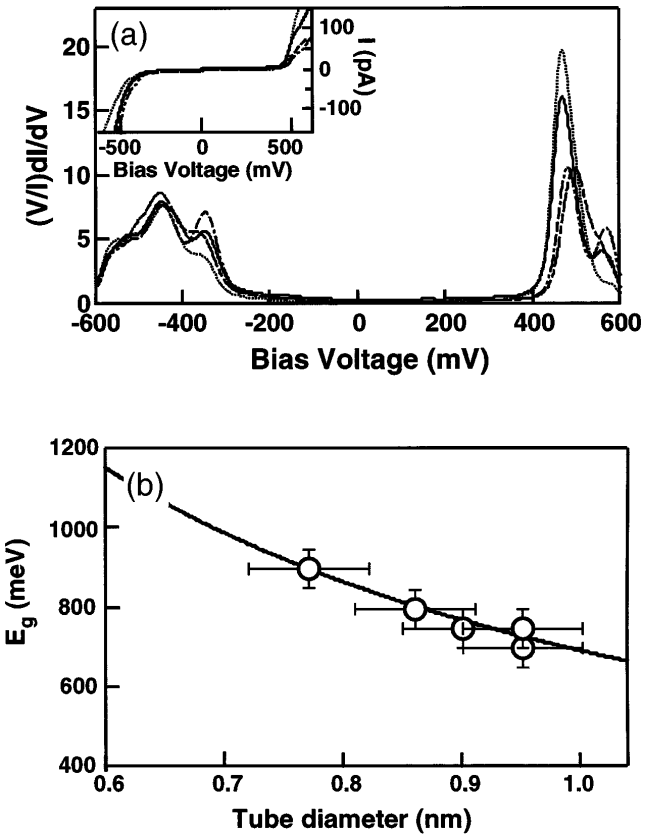

FIG. 8. (a) Calculated normalized conductance and measured *I-V* (inset) data recorded on the SWNT in Fig. 5(a) at the positions indicated by symbols: (—)/(●); (···)/(■); (- - -)/(▲); and (− · ·)/(◆). (b) Summary of energy gap (E_g) versus tube diameter data. The solid line corresponds to $E_g = 2\gamma_0 a_{C-C}/d$ with $\gamma_0 = 2.45$ eV. Adapted from Ref. 28.

of the energy gaps (E_g) obtained from these measurements for tubes with diameters between 0.6 and 1.1 nm is shown in Fig. 8(b). These results exhibit the expected[1,7,10] 1/diameter (d) dependence, and can be fit to $E_g = 2\gamma_0 a_{C-C}/d$, where $\gamma_0 = 2.45$ eV is the nearest-neighbor overlap integral and a_{C-C} is the C−C distance [Fig. 8(b)]. Significantly, this value of γ_0 is in good agreement with the 2.5 eV value determined from calculations,[1] and provides an additional consistency check in this work.

It is also important to recognize issues that require further work in the future. For example, in these and other studies,[28,29] the effect of coupling between the substrate and the nanotube on the observed electronic properties has been neglected. The delocalized Au wavefunction may, however, overlap with that of the SWNT's and shift the electronic energy levels; such behavior has been reported previously for C_{60} on Au(111) surfaces.[35,36] In our data, an asymmetry is often detected in the *I-V* curves around zero bias voltage. This asymmetry indicates that there has been charge transfer

from the Au substate to a SWNT. We believe that the perturbation of the nanotube electronic properties by the Au substrate is small in most cases, although explicit tests should be carried out in the future (e.g., comparing measurements on distinct substrates). SWNT-substrate coupling can, however, be quite strong at the ends of the tubes (where the nanotube wavefunctions are localized), as shown in Fig. 9. These data show that the images of the tube change dramatically depending on the bias voltage; that is, at positive bias the end of the tube appears to disappear into the Au(111) substrate. On the one hand, these results indicate clearly that care must be taken in analyzing data recorded from SWNT regions coupled strongly to substrate. Alternatively, a better understanding of how to controllably achieve strongly coupled tubes could impact significantly transport measurements and the development of nanodevices based on SWNT's.

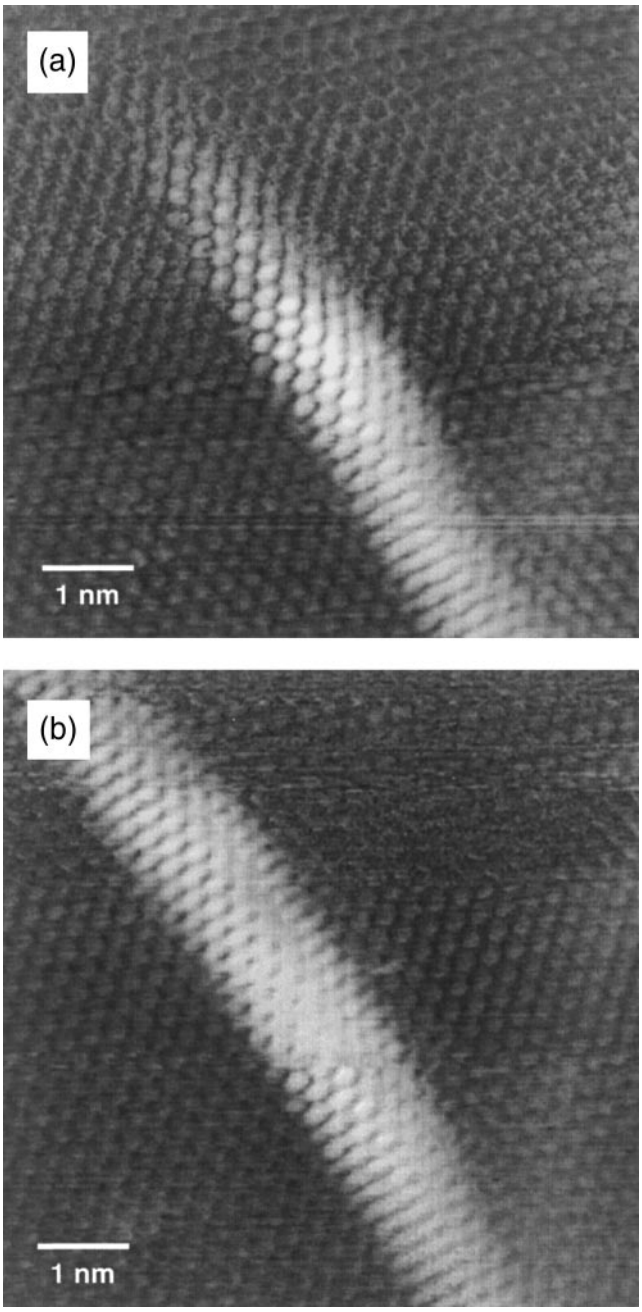

FIG. 9. Constant current STM images recorded at the end of an isolated SWNT in the constant current mode (120 pA). The bias voltage in (a) was +250 mV and that in (b) was −250 mV. The atomic structure of the SWNT and the Au(111) substrate surface are visible in both images.

IV. CONCLUSIONS

Scanning tunneling microscopy and spectroscopy have been used to characterize the atomic structure and tunneling density of states of individual SWNT's and ropes containing many SWNT's. In general, analyses of atomically resolved SWNT images show that the nanotubes consist of a wide range of diameters and helicities with no one structure clearly dominant. Recent experiments and work in progress indicate, however, that cutting and etching SWNT ropes may lead to samples enriched in armchair tubes. Tunneling spectroscopy measurements made simultaneously on atomically resolved SWNT's exhibit semiconducting and metallic behavior that depend predictably on helicity and diameter. In addition, the band gaps of the semiconducting tubes were also found to depend inversely on diameter with an overlap integral value which agrees with calculations, and upon extending the bias range, 1D van Hove singularities are observed in the normalized conductance. In the future, work will be needed to understand in greater detail a number of important issues, including the magnitude of curvature induced mixing and nanotube-substrate coupling.

ACKNOWLEDGMENTS

We thank J. Liu and R. E. Smalley for helpful discussions and samples, and D. Vezenov for help with the Au deposition. T. W. O. acknowledges fellowship support from the NSF. This work was supported by the NSF Division of Materials Research.

REFERENCES

1. M. S. Dresselhaus, G. Dresselhaus, and P. C. Eklund, in *Science of Fullerenes and Carbon Nanotubes* (Academic, San Diego, CA, 1996).
2. B. I. Yakobsen and R. E. Smalley, Am. Sci. **85**, 324 (1997).
3. M. S. Dresselhaus, Nature (London) **391**, 19 (1998).
4. M. M. J. Treacy, T. W. Ebbesen, and J. M. Gibson, Nature (London) **381**, 678 (1996).
5. E. W. Wong, P. E. Sheehan, and C. M. Lieber, Science **277**, 1971 (1997).
6. J. W. Mintmire, B. I. Dunlap, and C. T. White, Phys. Rev. Lett. **68**, 631 (1992).
7. N. Hamada, S. Sawada, and A. Oshiyama, Phys. Rev. Lett. **68**, 1579 (1992).

8. R. Saito, M. Fujita, G. Dresselhaus, and M. S. Dresselhaus, Appl. Phys. Lett. **60**, 2204 (1992).
9. R. Saito, M. Fujita, G. Dresselhaus, and M. S. Dresselhaus, Phys. Rev. B **46**, 1804 (1992).
10. C. T. White, D. H. Robertson, and J. W. Mintmire, Phys. Rev. B **47**, 5485 (1993).
11. L. Chico, V. H. Crespi, L. X. Benedict, S. G. Louie, and M. L. Cohen, Phys. Rev. Lett. **76**, 971 (1996).
12. R. Saito, G. Dresselhaus, and M. S. Dresselhaus, Phys. Rev. B **53**, 2044 (1996).
13. J-C. Charlier, T. W. Ebbesen, and Ph. Lambin, Phys. Rev. B **53**, 11 108 (1996).
14. V. H. Crespi, M. L. Cohen, and A. Rubio, Phys. Rev. Lett. **79**, 2093 (1997).
15. C. Kane, L. Balents, and M. P. A. Fisher, Phys. Rev. Lett. **79**, 5086 (1997).
16. M. Bockrath, D. H. Cobden, P. L. McEuen, N. G. Chopra, A. Zettl, A. Thess, and R. E. Smalley, Science **275**, 1922 (1997).
17. S. J. Tans, M. H. Devoret, H. Dai, A. Thess, R. E. Smalley, L. J. Geerligs, and C. Dekker, Nature (London) **386**, 474 (1997).
18. M. Ge and K. Sattler, Science **260**, 515 (1993).
19. Z. Zhang and C. M. Lieber, Appl. Phys. Lett. **62**, 2972 (1993).
20. C. H. Olk and J. P. Heremans, J. Mater. Res. **9**, 259 (1994).
21. M. Ge and K. Sattler, Appl. Phys. Lett. **65**, 2284 (1994).
22. S. Zie, N. Li, Z. Zhang, W. Liu, G. Wang, S. Qin, and C. Fu, J. Mater. Sci. **30**, 2291 (1995).
23. N. Lin, J. Ding, S. Yang, and N. Cue, Carbon **34**, 1295 (1996).
24. D. L. Carroll, P. Redlich, P. M. Ajayan, J. C. Charlier, X. Blase, A. De Vita, and R. Car, Phys. Rev. Lett. **78**, 2811–2814 (1997).
25. A. Thess, R. Lee, P. Nikolaev, H. Dai, P Petit, J. Robert, C. Xu, Y. H. Lee, S. G. Kim, A. G. Rinzler, D. T. Colbert, G. E. Scuseria, D. Tomanek, J. E. Fischer, and R. E. Smalley, Science **273**, 483–487 (1996).
26. C. Journet, W. K. Maser, P. Bernier, A. Loiseau, M. Lamy de la Chapelle, S. Lefrant, P. Deniard, R. Lee, and J. E. Fischer, Nature (London) **388**, 756 (1997).
27. J. Liu, A. G. Rinzler, H. Dai, J. H. Hafner, R. K. Bradley, A. Lu, T. Iverson, K. Shelimov, C. B. Huffman, F. Rodriguez-Macias, P. J. Boul, D. T. Colbert, and R. E. Smalley, unpublished.
28. T. W. Odom, J-L. Huang, P. Kim, and C. M. Lieber, Nature (London) **391**, 62 (1998).
29. J. W. G. Wildoer, L. C. Venema, A. G. Rinzler, R. E. Smalley, and C. Dekker, Nature (London) **391**, 58, 1998).
30. J. A. Stroscio and R. M. Feenstra, in *Scanning Tunneling Microscopy*, edited by J. a. Stroscio and W. J. Kaiser (Academic, New York, 1993), p. 95.
31. M. P. Everson, R. C. Jaklevic, and W. Shen, J. Vac. Sci. Technol. A **8**, 3662 (1990).
32. A. M. Rao, E. Richter, S. Bandow, B. Chae, P. C. Eklund, K. A. Williams, S. Fang, K. R. Subbaswamy, M. Menon, A. Thess, and R. E. Smalley, Science **275**, 187 (1997).
33. T. W. Odom, J-L. Huang, J. Liu, P. Kim, R. E. Smalley, and C. M. Lieber, unpublished.
34. P. Kim, T. W. Odom, J-L. Huang, and C. M. Lieber, unpublished.
35. T. Chen, S. Howells, M. Gallagher, L. Yi, and D. Sarid, D. L. Lichtenberger, K. W. Nebesny, and C. D. Ray, J. Vac. Sci. Tech. B **10**, 170 (1992).
36. T. R. Ohno, Y. Chen, S. E. Harvey, G. H. Kroll, J. H. Weaver, R. E. Haufler, and R. E. Smalley, Phys. Rev. B **44**, 13 747 (1991).